研究成果の刊行に関する一覧表

書籍

著者氏名	論文タイトル名	書籍全体の編集者名	書籍名	出版社名	出版地	出版年	ページ
Saijo Y	Ultrasonic measurement of micro-acoustic properties of the biological soft materials.	Tribikram Kundu	*Advanced Ultrasonic Methods for Material Characterization*	ISTE	London	2007	89-113
西條芳文	第2章. 第4節. 4. 超音波顕微鏡による組織性状の可視化.	小川誠二、上野照剛	非侵襲・可視化技術ハンドブック	株式会社エヌティーエス	東京	2007	241-249

雑誌

発表者氏名	論文タイトル名	発表誌名	巻名	ページ	出版年
Saijo Y, Hozumi N, Kobayashi K, OkadaN, Santos Filho ED, Sasaki H, Yambe T, Tanaka M.	Ultrasonic tissue characterization of atherosclerosis by a speed-of-sound microscanning system.	*IEEE Trans Ultrason Ferroelectr Freq Control*	Vol. 54, No. 8	1571-1577	2007
Tanaka A, Saijo Y	Blood flow visualization of left atrial spontaneous echo contrast (SEC) using gradient based optical flow estimation.	*Conf Proc IEEE Eng Med Biol Soc*	Vol. 1	4500-3	2007
Shiraishi Y, Yambe T, Saijo Y, Sato F, Tanaka A, Yoshizawa M, Ogawa D, Wada Y, Itoh S, Sakata R, Park Y, Uematsu M, Umezu M, Fujimoto T, Masumoto N, Liu H, Baba A, Konno S, Nitta S, Imachi K, Tabayashi K, Sasada H, Homma D	Morphological approach for the functional improvement of an artificial myocardial assist device using shape memory alloy fibres.	*Conf Proc IEEE Eng Med Biol Soc*	Vol. 1	3974-7	2007

Saijo Y, Hozumi N, Kobayashi K, Okada N, Ishiguro T, Hagiwara Y, Dos Santos Filho E, Yambe T	Ultrasound speed and impedance microscopy for in vivo imaging.	*Conf Proc IEEE Eng Med Biol Soc*	Vol. 1	1350-3	2007
Liu H, Luo Y, Higa M, Zhang X, Saijo Y, Shiraishi Y, Sekine K, Yambe T	Biochemical evaluation of an artificial anal sphincter made from shape memory alloys.	*J Artif Organs*	Vol. 10	223-227	2007
Saijo Y, Hagiwara Y, Kobayashi K, Okada N, Tanaka A, Hozumi N, Tomihata K	B-mode and C-mode imaging of regenerated 3D skin model with 100 MHz ultrasound.	*Proc 2007 IEEE International Ultrasonics Sysmposium*		244-247	2007
Hozumi N, Nakao A, Terauchi S, Nagao M, Yoshida S, Kobayashi K, Yamamoto S, Saijo Y	Precise calibration for biological acoustic impedance microscope.	*Proc 2007 IEEE International Ultrasonics Sysmposium*		801-804	2007
Okazaki T, Ebihara S, Asada M, Yamanda S, Saijo Y, Shiraishi Y, Ebihara T, Niu K, Mei H, Arai H, Yambe T	Macrophage colony-stimulating factor improves cardiac function after ischemic injury by inducing vascular endothelial growth factor production and survival of cardiomyocytes.	*Am J Pathol*	Vol. 171, No. 4	1093-1103	2007
Santos Filho E, Saijo Y, Tanaka A, Yambe T, Yoshizawa M	Fractal dimension of 40 MHz intravascular ultrasound radio frequency signals.	*Ultrasonics*		[Epub ahead of print]	2007
Santos Filho E, Saijo Y, Tanaka A, Yoshizawa M	Detection and quantification of calcifications in intravascular ultrasound images by automatic thresholding.	*Ultrasound Med Biol*	Vol. 34, No. 1	160-165	2008

研究成果の刊行物・別刷

Ultrasonic Tissue Characterization of Atherosclerosis by a Speed-of-Sound Microscanning System

Yoshifumi Saijo, Esmeraldo Santos Filho, Hidehiko Sasaki, Tomoyuki Yambe, Motonao Tanaka, Naohiro Hozumi, *Member, IEEE*, Kazuto Kobayashi, and Nagaya Okada

***Abstract*—We have been developing a scanning acoustic microscope (SAM) system for medicine and biology featuring quantitative measurement of ultrasonic parameters of soft tissues. In the present study, we propose a new concept sound speed microscopy that can measure the thickness and speed of sound in the tissue using fast Fourier transform of a single pulsed wave instead of burst waves used in conventional SAM systems. Two coronary arteries were frozen and sectioned approximately 10 μm in thickness. They were mounted on glass slides without cover slips. The scanning time of a frame with 300 × 300 pixels was 90 s and two-dimensional distribution of speed of sound was obtained. The speed of sound was 1680 ± 30 m/s in the thickened intima with collagen fiber, 1520 ± 8 m/s in the lipid deposition underlying the fibrous cap, and 1810 ± 25 m/s in a calcified lesion in the intima. These basic measurements will help in the understanding of echo intensity and pattern in intravascular ultrasound images.**

I. Introduction

We have been developing a scanning acoustic microscopy (SAM) system for biomedical use since the 1980s [1]–[10]. We have been investigating the acoustic properties of various organs and disease states by using this SAM system. In the areas of medicine and biology, SAM has three main objectives. First, SAM is useful for intraoperative pathological examination because it does not require special staining. Second, SAM provides basic data for understanding lower-frequency medical ultrasound images such as in echocardiography or intravascular ultrasound. Third, SAM can be used to assess the biomechanics of tissues and cells at a microscopic level. The originality of the previous SAM system of Tohoku University lies in providing quantitative values of attenuation and speed of sound in thin slices of soft tissue. Although the system may still be in use, it was constructed using precise handcrafted technologies and analog signal acquisition circuits. In addition, the previous system needed repeated acquisitions for calculation of quantitative values because it used burst waves of different frequencies.

Recently, we proposed a prototype of a speed-of-sound microscanning system using a single pulsed wave instead of the burst waves used in conventional SAM systems [11]. In the present study, we constructed a compact speed-of-sound microscanning system and evaluated the system performance by measuring normal and atherosclerotic coronary arteries.

Manuscript received April 30, 2006; accepted October 18, 2006. This study was supported by Grants-in-Aid for Scientific Research (Scientific Research (B) 15300178, Scientific Research (B) 15360217) from the Japan Society for the Promotion of Science and Health and Labor Sciences Research Grants from the Ministry of Health, Labor and Welfare for the Research on Advanced Medical Technology (H17-Nano-001).

Y. Saijo, E. D. Santos Filho, H. Sasaki, T. Yambe, and M. Tanaka are with the Department of Medical Engineering and Cardiology, Institute of Development, Aging and Cancer, Tohoku University, Aoba-ku, Sendai 980-8575, Japan (e-mail: saijo@idac.tohoku.ac.jp).

N. Hozumi is with the Department of Electrical and Electronic Engineering, Aichi Institute of Technology, Yakusa, Toyota, 470-0392, Japan.

K. Kobayashi and N. Okada are with the Research and Development Headquarters, Honda Electronics Co. Ltd., Oiwa-cho, Toyohashi, 441-3193, Japan.

Digital Object Identifier 10.1109/TUFFC.2007.427

II. Methods

A. Principle of Acoustic Microscopy

In order to realize high-resolution imaging, the speed-of-sound microscanning system was designed to transmit and receive wide-frequency ultrasound up to 500 MHz. In our previous SAM system with burst waves, the central frequency was changed in 10-MHz steps between 100 and 200 MHz to obtain frequency-dependent characteristics of the amplitude and phase of the received signal. The spectrum for calculation of the thickness and sound speed of the material was approximated with the frequency-dependent characteristics. Fig. 1 shows an example of the frequency-dependent characteristics of the amplitude (a) and the phase (b).

Our previous SAM system was able to visualize quantitative acoustic properties of stable materials but it was not suitable for living biological materials because it required several measurements with different frequencies on the same position. Besides, the frequency range was not suitable for visualization of living cells because the spatial resolution was approximately 10 microns.

In the present method, a pulsed ultrasound with broadband frequency is captured in a time domain and the frequency domain analysis is performed by software. The data acquisition of each sampling point takes longer than with the conventional SAM, but only a single measurement on the observation plane is required in the proposed method.

First, considering the frequency characteristics of the high-frequency ultrasound transducer, the appropriate

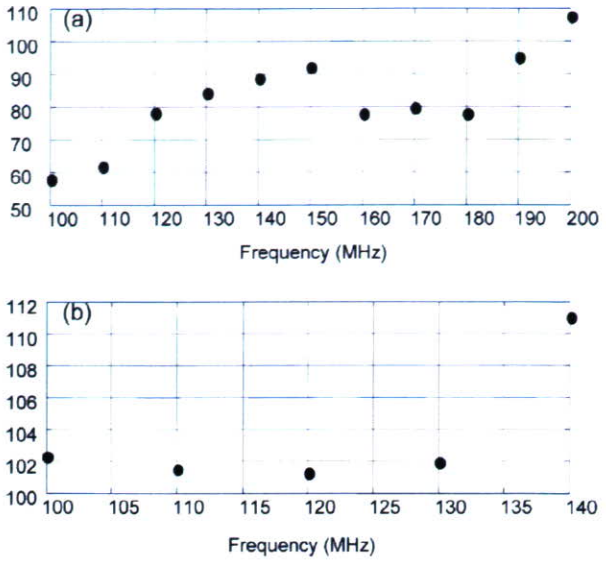

Fig. 1. Frequency-dependent characteristics of amplitude (a) and phase (b) obtained with our previous SAM system.

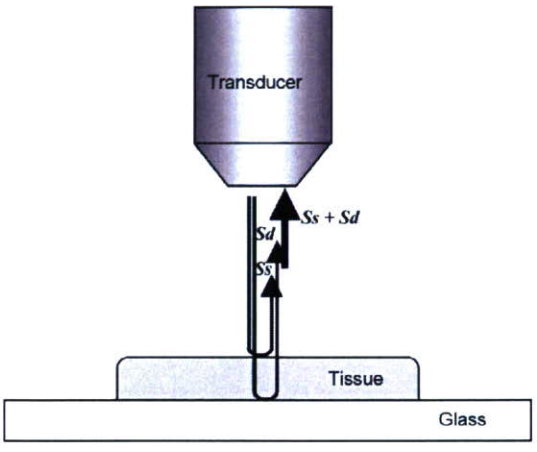

Fig. 2. Principle of quantitative measurement of acoustic properties by SAM.

pulse waveform and measurement system was designed. In order to analyze the signal in a frequency domain, the pulse width should be as short as possible and the pulse waveform should not contain many reverbs. Second, for realization of a compact system, integration of the scanner and signal acquisition was considered to design the whole acoustic microscope system.

Fig. 2 shows the principle of a scanning acoustic microscope. The soft biological material is attached to a substrate. Normal glass slides or high-molecular polymer materials used in dishes for cell culture can be used as the substrates. The biological material is sectioned at an appropriate thickness to separate the reflections from the tissue surface and from the interface between tissue and substrate. Single-layered cultured cells are also appropriate objects for SAM. The ultrasound is transmitted through a coupling medium and focused on the surface of the substrate. Transmitted ultrasound is reflected at both the surface of the biological material (S_s) and the interface between the biological material and the substrate (S_d). The transducer receives the sum of these two reflections. The interference of these two reflections is determined by the acoustic properties of the biological material. The determinants of the interference in the frequency (x-axis) are thickness and sound speed of the sample. The determinant of the interference of the intensity (y-axis) is the amplitude of the surface reflection and the attenuation of ultrasound propagating through the tissue. The concept of quantitative measurement of sound speed is based on the analysis of the interference frequency-dependent characteristics. In our previous SAM system, the frequency-dependent characteristics were obtained by serial measurements. The proposed sound speed SAM obtains the frequency-dependent characteristics by fast Fourier transform of a single broadband pulse.

B. Design of the Speed of Sound Microscanning System

An electric impulse was generated by a high-speed switching semiconductor. The start of the electric pulse was within 400 ps, the pulse width was 2 ns, and the pulse voltage was 40 V. Fig. 3(a) is the waveform of the electric pulse and Fig. 3(b) is the spectrum of the pulse. The spectrum extends to 500 MHz. The electric pulse was input to a transducer with a sapphire rod as an acoustic lens and with a central frequency of 300 MHz. Fig. 3(c) is the reflected wave form from the surface of the substrate. The ultrasonic pulse was changed from the electric pulse due to the frequency-dependent characteristics of the transducer, and it contained some oscillation components. The ultrasound spectrum is broad enough to cover 100–500 MHz [Fig. 3(d)].

The original electric pulse was almost an impulse, but the transmitted ultrasound contained oscillation components because of the thickness of the piezoelectric material of the transducer. The reflected wave also contained two components of reflections from the surface of the tissue and the interface between the tissue and the substrate. The waveform from the tissue and the glass was standardized by a reflection from the glass.

Fig. 3(e) shows the response to a singlet after this compensation. The reflections from the surface (front) and the interface (rear) are clearly seen in the waveform. These two peaks were separated by using proper window functions. The window function was originally a Gaussian function with 1 as its peak value, but the peak was flattened by splitting it at the peak point and inserting 1 with an appropriate length. Intensity and phase spectra of these separated waveforms were then calculated by Fourier transform.

Fig. 4 shows a block diagram of the speed-of-sound microscanning system for biological tissue characterization. A single ultrasound pulse with a pulse width of 2 ns was emitted and received by the same transducer above the specimen. The aperture diameter of the transducer was

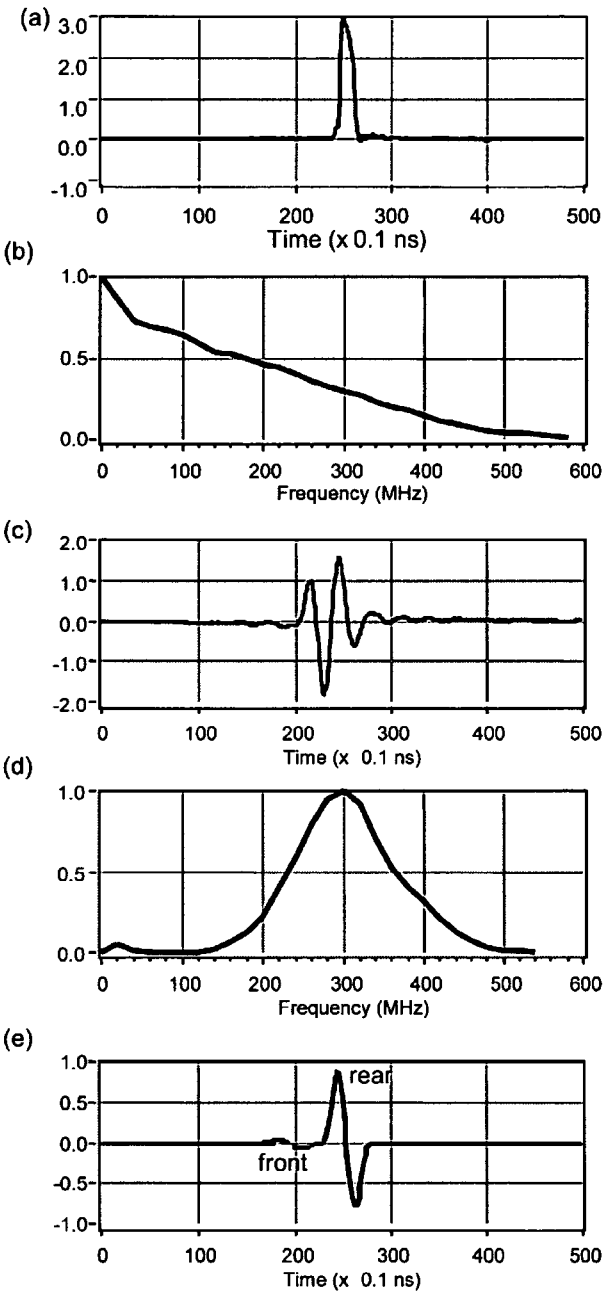

Fig. 3. (a) Waveform of the electric pulse; (b) the spectrum of the pulse; (c) the reflected wave form from the surface of the substrate; (d) ultrasound spectrum of the transducer; and (e) response to a singlet after standardization by a reflection from the glass. The reflections from the tissue surface (front) and the interface between the tissue and glass (rear) were separated in (e). The y-axis of each figure is normalized intensity (arbitrary units).

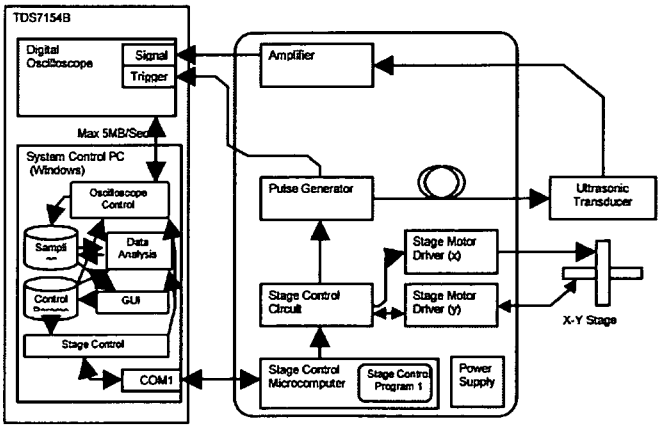

Fig. 4. Block diagram of sound speed microscopy.

1.2 mm, and the focal length was 1.5 mm. The central frequency was 300 MHz, the bandwidth was 100–500 MHz, and the pulse repetition rate was 10 kHz. The diameter of the focal spot was estimated to be 6.5 μm at 500 MHz by taking into account the focal distance and the sectional area of the transducer. Saline was used as the coupling medium between the transducer and the specimen. The reflections from the tissue surface and those from the interface between the tissue and glass were received by the transducer and were introduced into a Windows-based PC (Pentium D, 3.0 GHz, 2GB RAM, 250GB HDD) via a digital oscilloscope (Tektronix TDS7154B, Beaverton, OR). The frequency range was 1 GHz, and the sampling rate was 20 GS/s. Four consecutive values of the time taken for a pulse response were averaged in order to reduce random noise.

The transducer was mounted on an X-Y stage with a microcomputer board that was driven by the PC through an RS-232C interface. Both the X-scan and the Y-scan were driven by linear servo motors and the position was detected by an encoder. The scan was controlled to reduce the effects of acceleration at the start and deceleration at the end of the X-scan. Finally, two-dimensional distributions of ultrasonic intensity, speed of sound, attenuation coefficient, and thickness of a specimen measuring 2.4 × 2.4 mm were visualized using 300 × 300 pixels. The total scanning time was 90 s.

C. Signal Analysis

Denoting the standardized phase of the reflection wave at the tissue surface as ϕ_{front}, and the standardized phase at the interference between the tissue and the substrate as ϕ_{rear},

$$2\pi f \times \frac{2d}{c_o} = \phi_{\text{front}}, \tag{1}$$

$$2\pi f \times 2d\left(\frac{1}{c_o} - \frac{1}{c}\right) = \phi_{\text{rear}}, \tag{2}$$

where d is the tissue thickness, c_o is the sound speed in coupling medium, and c is the sound speed in the tissue.

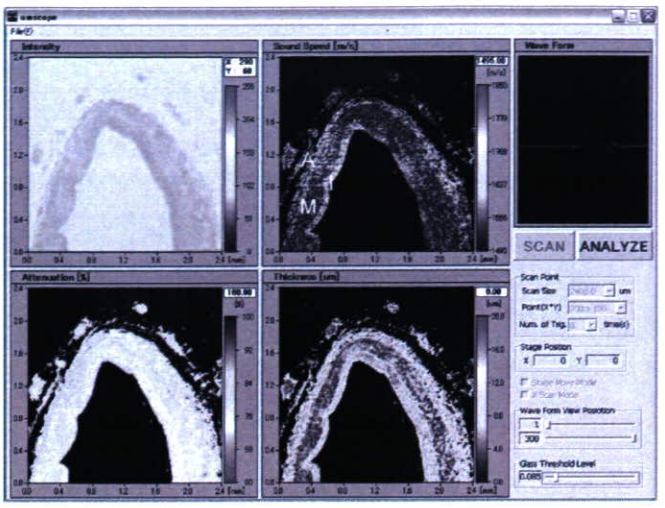

Fig. 5. PC window of speed of sound microscopy showing a normal coronary artery. Upper left: amplitude image; upper right: speed of sound image; lower left: attenuation image; and lower right: thickness. I: Intima; M: media; A: adventitia.

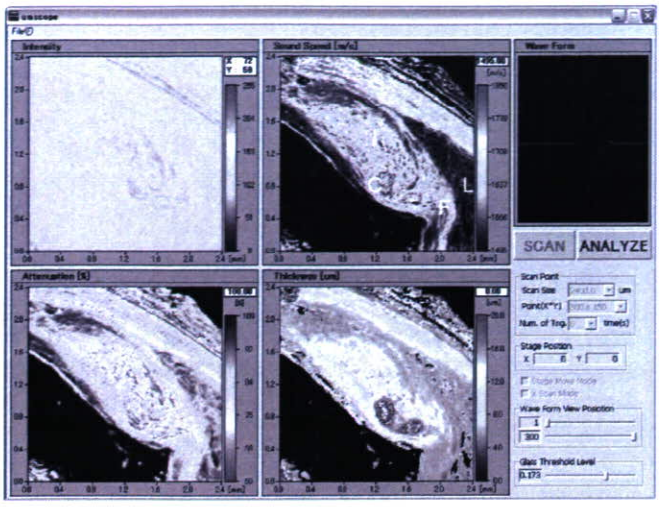

Fig. 6. PC window of speed-of-sound microscopy showing an atherosclerotic coronary artery. Upper left: amplitude image; upper right: speed of sound image; lower left: attenuation image; and lower right: thickness. I: intima; C: calcified lesion; F: fibrous cap; L: lipid.

Thickness is obtained as

$$d = \frac{c_o}{4\pi f}\phi_{\text{front}}. \tag{3}$$

Finally, sound speed is calculated as

$$c = \left(\frac{1}{c_o} - \frac{\phi_{\text{rear}}}{4\pi f d}\right)^{-1}. \tag{4}$$

After determination of the thickness, attenuation of ultrasound was then calculated by dividing the amplitude by the thickness and the frequency.

D. Tissue Preparation

Normal and atherosclerotic human coronary arteries were obtained from autopsy. The specimens were rinsed in phosphate buffer saline (PBS) and immersed in 10% to 30% sucrose solutions. Then the specimens were embedded in optimal cutting temperature (OCT) compound and rapidly frozen by liquid nitrogen at −20°C. The specimens were sliced at approximately 10 microns by a cryostat and mounted on silane-coated glass slides.

III. Results

Fig. 5 shows a PC window of the speed-of-sound microscanning system. The upper left is an intensity image, the upper right is a sound speed image, the lower left is an attenuation image, and the lower right is the thickness distribution of the normal coronary artery. In the present case, the attenuation image of the system means the intensity divided by the thickness. It is not quantitatively calculated as the attenuation coefficient. The intima was thin, and the sound speed was 1600 ± 20 m/s in the intima (I), 1560 ± 18 m/s in the medium (M), and 1590 ± 22 m/s in the adventitia (A). The thickness was 7.2 ± 0.1 μm in the intima, 4.8 ± 0.2 μm in the medium and 7.2 ± 0.1 μm in the adventitia. In qualitative analysis, the attenuation of the medium was slightly lower than that of either the intima or the adventitia.

Fig. 6 is an atherosclerotic coronary artery. The sound speed was 1680 ± 30 m/s in the thickened intima (I) with collagen fiber, 1520 ± 8 m/s in lipid deposition (L) underlying the fibrous cap (F), and 1810 ± 25 m/s in the calcified lesion (C) in the intima. The thickness was 11.8 ± 0.1 μm in the intima, 11.6 ± 0.2 μm in the medium and 14.8 ± 0.1 μm in the lipid deposition. In qualitative analysis, the attenuation of the calcified lesion was high and the attenuation in lipid deposition was low.

IV. Discussion

In the present study, speed of sound in the excised human coronary arteries was measured with the specially developed microscanning system. The results showed that the speed of sound in the intima and the adventitia, mainly consisting of collagen fiber, had higher values than that of the medium, mainly consisting of vascular smooth muscle. The difference of acoustic properties may lead to the classical three-layered appearance of a normal coronary artery in clinical intravascular ultrasound (IVUS) imaging. The findings indicate that the echo intensity is determined by the difference of acoustic impedance between neighboring layers because the specific acoustic impedance is the product of the speed of sound and the density. The distribution and the structure of materials with different acoustic properties may also contribute to the echo pattern in IVUS imaging.

The thick fibrous cap, consisting of collagen fiber in an atherosclerotic plaque, showed higher values of speed of

sound and attenuation than did normal medium. Generally, absorption and scattering are the two main factors of attenuation of ultrasound. Thus, the high scattering within the thickened intima or calcified lesion may lead to the high intensity echo in the clinical IVUS imaging. The region of lipid deposition showed low values of speed of sound. These values explain the low echo in the same manner as for renal cysts containing water-like fluid. Besides the absolute low values, the homogeneity of acoustic properties within the lipid pool may lead to the low scattering and consequently a lipid pool shows a low-intensity echo.

As ultrasound has the character of an elastic wave, ultrasound itself is closely related to the mechanical properties of tissues. The sound speed in a solid medium may be taken as

$$c = \sqrt{\frac{E(1-\sigma)}{\rho(1+\sigma)(1-2\sigma)}} \cdots, \tag{5}$$

where c is the speed of sound, E is the Young's elastic modulus, ρ is the density, and σ is the Poisson's ratio. The Poisson's ratio in biological soft materials is assumed to be nearly 0.5 and the density of these vary 3% [4]. Although these simple assumptions are not to be applied precisely, the information on the relative two-dimensional elasticity distribution can be assessed by sound speed image. A high value of sound speed means high elasticity of collagen which is the main component of the intimal thickening. Lipid is the main component of the lucent echogeneicity plaque, and the elasticity is low. The present study proved that the tissue component in the "hard plaque" was really hard and the component of "soft plaque" was really soft. Also, the intima mainly consisting of fibrotic tissues was harder than the normal intima-medium complex. The difference in the elasticity may explain why intimal tear often occurred at the junction of the thinnest plaque and adjacent normal arterial wall [12], [13]. Acoustic microscopy imaging, especially the sound speed image, is the interpretation of elasticity mapping, and it may also help in the understanding of the "elastography" [14] imaging of atherosclerotic plaques from a mechanical point of view.

There have been some time-resolved acoustic microscope systems [15], [16]. The most important feature of our sound speed microscope is that the system calculates the speed of sound and the thickness by frequency-domain analysis of the interference between the reflections from the tissue surface and from the interface between the tissue and glass. However, the error of the sound speed value is 15 m/s by the algorithm [17]. Besides, the system is not able to measure the speed of sound when the surface reflection is weak or the thickness is thinner than 3 μm because the two reflections cannot be separated.

V. Conclusions

An acoustic microscope system that can measure the sound speed of thin slices of biological material was developed. It is a unique acoustic microscope because it uses a single pulse and the Fourier transform to calculate the sound speed and the thickness at all measuring points. Although the data acquisition time of a single frame was greater than that in conventional SAM, the total time required for calculation was significantly shorter. The acoustic microscope system can be applied to intraoperative pathological examination, basic data for understanding lower-frequency medical ultrasound images, and assessment of biomechanics of tissues and cells at a microscopic level.

References

[1] M. Tanaka, H. Okawai, N. Chubachi, J. Kushibiki, and T. Sannomiya, "Propagation properties of ultrasound in acoustic microscopy through a double-layered specimen consisting of thin biological tissue and its holder," *Jpn. J. Appl. Phys.*, vol. 23, pp. 197–199, 1984.

[2] Y. Saijo, M. Tanaka, H. Okawai, and F. Dunn, "The ultrasonic properties of gastric cancer tissues obtained with a scanning acoustic microscope system," *Ultrasound Med. Biol.*, vol. 17, pp. 709–714, 1991.

[3] H. Sasaki, M. Tanaka, Y. Saijo, H. Okawai, Y. Terasawa, S. Nitta, and K. Suzuki, "Ultrasonic tissue characterization of renal cell carcinoma tissue," *Nephron*, vol. 74, pp. 125–130, 1996.

[4] Y. Saijo, M. Tanaka, H. Okawai, H. Sasaki, S. Nitta, and F. Dunn, "Ultrasonic tissue characterization of infarcted myocardium by scanning acoustic microscopy," *Ultrasound Med. Biol.*, vol. 23, pp. 77–85, 1997.

[5] Y. Saijo, H. Sasaki, H. Okawai, S. Nitta, and M. Tanaka, "Acoustic properties of atherosclerosis of human aorta obtained with high-frequency ultrasound," *Ultrasound Med. Biol.*, vol. 24, pp. 1061–1064, 1998.

[6] Y. Saijo, H. Sasaki, M. Sato, S. Nitta, and M. Tanaka, "Visualization of human umbilical vein endothelial cells by acoustic microscopy," *Ultrasonics*, vol. 38, pp. 396–399, 2000.

[7] Y. Saijo, T. Ohashi, H. Sasaki, M. Sato, C. S. Jorgensen, and S. Nitta, "Application of scanning acoustic microscopy for assessing stress distribution in atherosclerotic plaque," *Ann. Biomed. Eng.*, vol. 29, pp. 1048–1053, 2001.

[8] H. Sasaki, Y. Saijo, M. Tanaka, and S. Nitta, "Influence of tissue preparation on the acoustic properties of tissue sections at high frequencies," *Ultrasound Med. Biol.*, vol. 29, pp. 1367–1372, 2003.

[9] Y. Saijo, T. Miyakawa, H. Sasaki, M. Tanaka, and S. Nitta, "Acoustic properties of aortic aneurysm obtained with scanning acoustic microscopy," *Ultrasonics*, vol. 42, pp. 695–698, 2004.

[10] H. Sano, Y. Saijo, and S. Kokubun, "Material properties of the supraspinatus tendon at its insertion—A measurement with the scanning acoustic microscopy," *J. Musculoskeletal Res.*, vol. 8, pp. 29–34, 2004.

[11] N. Hozumi, R. Yamashita, C. K. Lee, M. Nagao, K. Kobayashi, Y. Saijo, M. Tanaka, N. Tanaka, and S. Ohtsuki, "Time-frequency analysis for pulse driven ultrasonic microscopy for biological tissue characterization," *Ultrasonics*, vol. 42, pp. 717–722, 2004.

[12] R. T. Lee and R. D. Kamm, "Vascular mechanics for the cardiologist," *J. Amer. Coll. Cardiol.*, vol. 23, pp. 1289–1295, 1994.

[13] A. Maehara, G. S. Mintz, A. B. Bui, M. T. Castagna, O. R. Walter, C. Pappas, E. E. Pinnow, A. D. Pichard, L. F. Satler, R. Waksman, W. O. Suddath, J. R. Laird , Jr., K. M. Kent, and N. J. Weissman, "Incidence, morphology, angiographic findings, and outcomes of intramural hematomas after percutaneous coronary interventions: An intravascular ultrasound study," *Circulation*, vol. 105, pp. 2037–2042, 2002.

[14] C. L. de Korte, G. Pasterkamp, A. F. van der Steen, H. A. Woutman, and N. Bom, "Characterization of plaque components with intravascular ultrasound elastography in human femoral and coronary arteries in vitro," *Circulation*, vol. 102, pp. 617–623, 2002.

[15] C. M. Daft and G. A. Briggs, "The elastic microstructure of various tissues," *J. Acoust. Soc. Amer.*, vol. 85, pp. 416–422, 1989.
[16] A. F. van der Steen, M. H. Cuypers, J. M. Thijssen, and P. C. de Wilde, "Influence of histochemical preparation on acoustic parameters of liver tissue: A 5-MHz study," *Ultrasound Med. Biol.*, vol. 17, pp. 879–891, 1991.
[17] N. Hozumi, "Development of sound speed acoustic microscopy for biological nano-imaging by picosecond evoked ultrasonic pulse," Research Accomplishment Report of Grants-in-aid for Scientific Research, 2006. (in Japanese)

Yoshifumi Saijo was born in Yokohama, Japan, on July 21, 1962. He received the M.D. and the Ph.D. degrees in 1988 and 1993, respectively, from Tohoku University.

He is currently an associate professor in the Department of Medical Engineering and Cardiology at the Institute of Development, Aging and Cancer, Tohoku University, and the Department of Cardiovascular Surgery, Tohoku University Hospital. His main research interests are assessment of biomechanics of cells and tissues by high-frequency ultrasound and clinical ultrasonic evaluation of cardiovascular system with intravascular ultrasound and transesophageal echocardiography. He received an award in 1997 for his outstanding research paper in *Ultrasound in Medicine and Biology*, the official journal of the World Federation of Ultrasound in Medicine and Biology. He is a member of the Japan Society of Ultrasonics in Medicine, the Japanese Society of Echocardiography, and the Japan Circulation Society.

Esmeraldo dos Santos Filho was born in 1971 in Sao Luis - MA, Brazil. He earned his bachelor and master degrees at the Federal University of Maranhao, in Brazil, in the years 1998 and 2000, respectively. In 2005, he earned his Ph.D. degree at Tohoku University in Japan.

During the academic year of 2001, he worked as a lecturer on digital systems at the Department of Electrical Engineering of the Federal University of Maranhao. Currently, he is a postdoctoral fellow of the Japan Association for Advancement of Medical Equipment at the Institute of Development, Aging, and Cancer, Tohoku University. His fields of interest are applications of artificial intelligence in biomedical image and signal processing. He is a member of the IEEE Signal Processing Society.

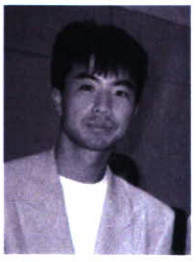

Hidehiko Sasaki received his M.D. degree from Yamagata University in 1990 and his Ph.D. degree from Tohoku University in 1996. He is currently Director of the Department of Cardiology at Miyagi Cardiovascular and Respiratory Center. His main research interest is acoustic microscopy evaluation of renal and cardiovascular diseases. He is a member of the Japan Society of Ultrasonics in Medicine and the Japanese Society of Interventional Cardiology.

Tomoyuki Yambe was born in May 7, 1959 in Sendai, Japan. He received the M.D. and the Ph.D. degrees in 1985 and 1989, respectively, from Tohoku University.

He is currently a professor in the Department of Medical Engineering and Cardiology at the Institute of Development, Aging and Cancer, Tohoku University. His main research interest includes development of artificial organs. He is a member of the Japanese Society for Artificial Organs.

Motonao Tanaka was born in Tokyo, Japan, on January 1, 1932. He received the M.D. and the Ph.D. degrees in 1958 and 1962, respectively, from Tohoku University. He was a professor in the Department of Medical Engineering and Cardiology at the Institute of Development, Aging and Cancer, Tohoku University from 1984 to 1996. He is currently Director of the Japan Anti-tuberculosis Association of Miyagi Prefecture. He invented one of the world's first B-mode echocardiographs in the early 60s. Since then he has been contributing to the development of medical ultrasound. He started developing acoustic microscopy for medicine and biology in 1985 and his current interest is "echodynamography" which enables visualization of stream lines and dynamic pressure distribution in heart chambers. He is a member of the Japan Society of Ultrasonics in Medicine, the Japanese Society of Echocardiography, and the Japan Circulation Society.

Naohiro Hozumi (M'94) was born in Kyoto, Japan, on April 2, 1957. He received his B.S., M.S., and Ph.D. degrees in 1981, 1983, and 1990, respectively, from Waseda University. He was employed at the Central Research Institute of Electric Power Industry (CRIEPI) from 1983 to 1999. He was an associate professor at Toyohashi University of Technology from 1999 to 2006. Since 2006, he has been a professor at Aichi Institute of Technology.

He has been engaged in research on insulating materials and diagnosis for high-voltage equipment, acoustic measurement for biological and medical applications, etc. He received awards in 1990 and 1999 from the IEE of Japan for his outstanding research papers. He is a member of IEEE, IEE of Japan, and the Acoustic Society of Japan.

Kazuto Kobayashi was born in Aichi, Japan, on June 8, 1952. He received his B.S. degree in electrical engineering from Shibaura Institute of Technology, Tokyo, Japan, in 1976.

He is currently Director of the Department of Research and Development at Honda Electronics Co. Ltd., Toyohashi, Japan. His research activities and interests include medical ultrasound imaging, signal processing, and high-frequency ultrasound transducers.

Nagaya Okada was born in Aichi, Japan, on January 27, 1964. He received the B.S. degree in electrical engineering from Shizuoka University, Shizuoka, Japan, in 1987, and the M.S. and Ph.D. degrees in electrical engineering from Shizuoka University, Shizuoka, Japan, in 1990 and 1993, respectively.

He is currently a manager of the Department of Research and Development at Honda Electronics Co. Ltd., Toyohashi, Japan. His research activities and interests include digital signal processing, ultrasound imaging and high-frequency ultrasound transducers.

Proceedings of the 29th Annual International
Conference of the IEEE EMBS
Cité Internationale, Lyon, France
August 23-26, 2007.

Blood Flow Visualization of Left Atrial Spontaneous Echo Contrast (SEC) Using gradient based optical flow estimation

Akira Tanaka, *Member, IEEE*, Yoshifumi Saijo, *Member, IEEE*

***Abstract*— Left atrial spontaneous echo contrast (SEC) is a dynamic smoke-like signal caused by an increased ultrasonic backscatter from aggregation of the cellular components of blood in the conditions of blood stases or low-velocity blood flow. SEC can be detected by transesophageal echocardiography (TEE). SEC has been proposed as an important cadioembolic source in patients with nonrheumatic arial fibrillation. Previous clinical investigations have shown that the presence of SEC is associated with a greater incidence of left atrial thrombi. Usually, the blood flow velocity is slower than lower limit of Doppler method in SEC. In order to diagnose SEC quantitatively, blood flow visualization in left atrium was performed using gradient based optical flow estimation.**

A movie of left atrium (LA) with SEC in a patient with atrial fibrillation was recorded by TEE with the frequency range of 4-7.5 MHz. Serial still frames were made from the movie. The 2-D flow vector map was calculated from consecutive frame images using gradient based optical flow estimation.

In the result of 2-D blood flow vector map, the low and swirling flow in LA were successfully visualized.

I. Introduction

LEFT atrial spontaneous echo contrast (SEC) is a dynamic smoke-like signal (Fig. 1). It caused by an increased ultrasonic backscatter from aggregation of the cellular components of blood in the conditions of blood stases or low-velocity blood flow [1][2]. SEC can be detected by transesophageal echocardiography (TEE). The most common condition predisposing to left atrial SEC are atrial fibrillation (AF) and mitral stenosis. Hence, SEC has been proposed as an important cardioembolic source in patients with nonrheumatic atrial fibrillation [1]-[3]. Previous clinical investigations have shown that the presence of SEC is associated with a greater incidence of left atrial thrombi [4][5]. Therefore, it is very important to diagnosis SEC in order to reduce the risk of thromboembolism. However, SEC is still described qualitatively [6][7].

The assessment of thromboembolic risk by measurement of left atrium (LA) appendage velocities using pulsed Doppler imaging during TEE in atrial fibrillation has become accepted [8]. LA appendage velocity may also represent LA appendage contractile function. Some studies have suggested that the conversion from atrial fibrillation to sinus rhythm may be predicted by evaluating LA appendage velocities before cardioversion [9]. Quantitative blood flow analysis in echocardiography has been mainly addressed using Doppler method. This approach, however, have disadvantages for SEC analysis. It has angle dependency because it only measures the velocity throughout the ultrasound beam direction. Besides, it cannot measure the low blood flow velocity which is slower than lower limit of Doppler method. Hence, it is difficult to visualize the swirling blood flow in left atrium (LA).

The aim of this study is visualization of retardant flow vector in LA.

Fig. 1. Spontaneous echo contrast of left atrium in transesophageal echocardiography

II. Methods

A. Clinical Data Acquisition

Transesophageal echocardiography was performed in a 70-year-old man with atrial fibrillation using a color Doppler system (SONOS5500, Philips, USA) and a 4-7.5MHz multiplane transducer (Omniplane 2, Hewlett Packerd, USA) under stable general anesthesia.

SEC was identified as a dynamic smokelike signal that swirled slowly in a circular pattern in the left atrium. The

Manuscript received April 16, 2007. This work was supported by Grants from New Energy and Industrial Technology Development organization (06001905-0)

Akira Tanaka is with Faculty of Symbiotic System Science, Fukushima University, Kanayagawa 1, Fukushima 960-1296, Japan. (e-mail: a-tanaka@iccc.org)

Yoshifumi Saijo is with Institute of Development, Aging and Cancer, Tohoku University, Seiryo-cho 4-1, Aoba-ku, Sendai 980-8575, Japan.

1-4244-0788-5/07/$20.00 ©2007 IEEE

presence of SEC was confirmed by decreasing the gain settings to exclude background noise artifact. The SEC video image was recorded as unarchived avi file into PC. The image size was 640x480 pixels (VGA) and frame rate was 30 fps.

B. Image Processing

The consecutive still frames in BMP format were made from the video file. As the preprocessing, the each frame denoised by Wiener filter [11].

In this study, to estimate blood flow vector of SEC, gradient-based optical flow estimation is used.

The Lucas-Kanade method [12] was applied as gradient-based optical flow estimation algorithm. This method is a simple yet powerful algorithm which has the advantage of less computational costs. The basic assumption in this algorithm is that the pixel intensities are constant along the motion trajectory. Hence, the displacement is calculated by computing a least squares estimate of the brightness constraint following equations for the pixels in the neighborhood.

$$uI_x + vI_y + I_t = 0 \tag{1}$$

where I_x, I_y and I_t represent the intensity gradients. (u, v) represents motion. The simplest method for computing the optical flow (u, v) is to integrate the image measurements in a neighborhood Ω of (x, y) and solve the following 2×2 linear equation using the least-squares estimation.

$$\sum_{\Omega}\begin{bmatrix} I_x^2 & I_xI_y \\ I_xI_y & I_y^2 \end{bmatrix}\begin{bmatrix} u \\ v \end{bmatrix} = -\sum_{\Omega}\begin{bmatrix} \sum I_xI_t \\ \sum I_xI_t \end{bmatrix} \tag{2}$$

After calculation of each motion vector, motion vectors ware imposed on B-mode image.

III. Result

Fig. 2 shows the blood flow vectors at mitral valve opening. It is observed that the blood in LA propagates from LA to mitral valve. Optical flow is calculated at all grid points, but the accuracy of vectors at the area where SEC is not observed or the intensity are low, e.g., part of aorta and left ventricle. Fig. 3 is the blood flow vectors of LA 60 msec (2 frames) after Fig.2. The blood flow vectors at mitral valve are very low and the propagation of blood toward into left ventricle is diminished. Optical flow represents not only SEC flow but also LA wall motion. Hence, Fig. 3 also indicates that the LA wall Besides, it is also indicate Fig. 4 shows the 2-D blood flow vectors at systole. Mitral valve is closed and the blood whiling is shown.

IV. Discussion

The LA appendage is known to be a principal site ob thrombus formation in AF. The blood flow is usually very slow and the flow pattern is complex like swirling flow in the LA appendage. In previous reports, immunoreactive von

Fig. 2 2-D blood flow vectors at mitral valve opening

Fig. 3 2-D blood flow vectors at 60msec after Fig. 2

Willebrand factor (vWF) in LA was correlated to wall shear stress caused by slow blood flow [13] and was correlated with the extent of platelet adhesion/aggregation leading to stroke [14],[15]. Thus, understanding LA flow state is important to predict and prevent atrial thrombus formation leading to stroke.

2-D velocity distribution in LA was successfully obtained with proposed method. the proposed flow distribution method has two major advantages. One is that the method

can detect very slow blood flow which cannot be detected by conventional Doppler method. In this study, the resolution of flow vector is 5.3 m/sec in case that the frame rate is 30 fps and image resolution is VGA and the resolution depends on the resolution of echo image and. Hence, it is easy to improve the flow resolution by using RF signal directly. The other advantage is that the method can visualize any directions of flow vectors in image plane while conventional Doppler method can only detect the flow along the ultrasonic beam.

The Lucas-Kanade method which is applied for the proposed flow distribution has a brightness constancy assumption. Usually, this assumption is almost satisfied because SEC consists mainly of very low flow components. This means, on the other hand, the proposed method cannot detect fast flow. Besides, the flow vector is not accurate in case that the dynamically change in the texture of SEC caused by the fast blood flow in vertical direction for the image plane. Hence, the accuracy of flow vector should be evaluated and visualized in each calculation of optical flow.

One of the limitations of the proposed method is that the method cannot detect the SEC flowing in three-dimensional space. This limitation may be overcome by deducing the velocity component orthogonal to the Doppler velocity with taking the law of conservation of mass (the equation of continuity) into consideration [16].

V. Conclusion

Because the presence of SEC is one of high risk signs of thrombosis leading to stroke, it is very important to diagnose the slow blood flow in LA with SEC. We applied the conventional gradient based optical flow estimation method to the flow distribution of SEC. The results indicate that the proposed method can represent low blood flow vector that cannot be detected by conventional Doppler method.

Optical flow vectors represent not only the slow blood flow in SEC but also the motion of heart muscle including atrial wall. Therefore, the proposed method may be able to contribute a specific diagnosis of AF or a risk evaluation for heat disease and stroke.

In future study, in order to solve the problem of a brightness constancy assumption, the evaluation and visualization of accuracy of each vector should be considered. Besides, another optical flow estimation method which does not need the assumption [17] should also be appled and compared with the proposed method.

Fig. 4. 2-D flow vectors at systole

References

[1] IW. Black, AP. Hopkins, LC. Lee, and WF Walsh, "Left atrial spontaneous echo contrast: a clinical and echocardiographic analysis", J Am Coll Cardiol, 18, pp. 398-404, 1991.

[2] LM. Tsai, JH. Chen, CJ. Fang, LJ. Lin, CM. Kwan, "Clinical implications of left atrial spontaneous echo contrast in nonrheumatic atrial fibrillation," Am J Cardiol., 70(3), pp. 327-331, Aug. 1992

[3] DYG. Leung, IW. Black, GB. Cranney, AP. Hopkins, WF. Walsh, "Prognostic implications of left atrial spontaneous echo contrast in nonvalvular atrial fibrillation," J Am Coll Cardiol., 24(3), pp. 755-762, Sep. 1994.

[4] R. Castello, AC. Pearson, AJ. Labovitz, "Prevalence and clinical implications of atrial spontaneous contrast in patients undergoing transesophageal echocardiography," Am J Cardiol., 65(16), pp. 1149-1153, May 1990.

[5] SL. Archer, LR. Kvernern, K. James, M. Ezekowitz, C. Gornick, "Does warfarin reduce the prevalence of left atrial thrombus in chronic atrial fibrillation? a double blind, placebo controlled study," Circulation, 84(suppl 2), II-693, 1991

[6] D. Fatkin, RP. Kelly, MP. Feneley, "Relations between left atrial appendage blood flow velocity, spontaneous echocardiographic contrast and thromboembolic risk in vivo," J Am Coll Cardiol, 23, pp. 961-969, 1994.

[7] E. Donal, H. Yamada, C. Leclercq, and D. Herpin, "The Left Atrial Appendage, a Small, Blind-Ended Structure: A Review of Its Echocardiographic Evaluation and Its Clinical Role," Chest, 128(3), pp. 1853-1862, Sep. 2005

[8] O. Kamp, PM. Verhost, RC. Welling, CA. Visser, "Importance of left atrial appendage flow as a predictor of thromboembolic events in patients with atrial fibriation," Eur. Heart J., 20, pp. 979-985, 1999.

[9] T. Tabata, T. Oki, A. Iuchi, H. Yamada, K. Manabe, K. Fukuda, M. Abe, N. Fukuda, S. Ito, "Evaluation of left atrial appendage function by measurement of changes in flow velocity patterns after electrical cardioversion in patients with isolated atrial fibrillation," Am J Cardiol., 79(5), pp. 615-620, Mar. 1997.

[10] T. Bartel, S. Müller, HJ. Nesser, S. Möhlenkamp, C. Bruch, R. Erbel, "Usefulness of motion patterns identified by tissue Doppler echocardiography for diagnosing various cardiac masses, particularly valvular vegetations," Am J Cardiol., 84, pp. 1428-1433, 1999.

[11] Lim, Jae S., "Two-Dimensional Signal and Image Processing," Englewood Cliffs, NJ, Prentice Hall, 1990, pp. 536-540.

[12] BD. Lucas and T. Kanade, "An iterative image registration technique with an application to stereo vision," Proc. of the 7th International Joint Conference on Articial Intelligence, 1981, pp. 674-679.

[13] H. M. Tsai, I. I. Sussman, R. L. Nagel. "Shear stress enhances the proteolysis of von Willebrand factor in normal plasma.", Blood. vol. 83, 1994, pp. 2171-2179.

[14] M. Fukuchi, J. Watanabe, K. Kumagai, Y. Katori, S. Baba, K. Fukuda, T. Yagi, A. Iguchi, H. Yokoyama, M. Miura, Y. Kagaya, S. Sato, K. Tabayashi, K. Shirato. "Increased von Willebrand Factor in the endocardium as a local predisposing factor for thrombogenesis in overloaded human atrial appendage.", J. Am. Coll. Cardiol. vol. 37, 2001, pp. 1436-1442.
[15] K. Kumagai, M. Fukuchi, J. Ohta, S. Baba, K. Oda, H. Akimoto, Y. Kagaya, J. Watanabe, K. Tabayashi, K. Shirato. "Expression of the von Willebrand factor in atrial endocardium is increased in atrial fibrillation depending on the extent of structural remodeling.", Circ. J. vol. 68, 2004, pp. 321-327.
[16] S. Ohtsuki, M. Tanaka. "Doppler pressure field deduced from the Doppler velocity field in an observation plane in a fluid.", Ultrasound Med. Biol. vol. 29, 2003, pp. 1431-1438.
[17] CH. Teng, SH. Lai, YS. Chen, WH. Hsu, "Accurate optical flow computation under non-uniform brightness variations", Computer Vision and Image Understanding, 97, 2005, pp. 315-346

Proceedings of the 29th Annual International
Conference of the IEEE EMBS
Cité Internationale, Lyon, France
August 23-26, 2007.

Morphological Approach for the Functional Improvement of an Artificial Myocardial Assist Device using Shape Memory Alloy Fibres

Y. Shiraishi, T. Yambe, Y. Saijo, F. Sato, A. Tanaka, M. Yoshizawa, D. Ogawa, *Member, IEEE*
Y. Wada, S. Itoh, R. Sakata, Y. Park, M. Uematsu, M. Umezu, T. Fujimoto, N. Masumoto, H. Liu,
A. Baba, S. Konno, S. Nitta, K. Imachi, K. Tabayashi, H. Sasada and D. Homma

***Abstract*— The authors have been developing a mechano-electric artificial myocardial assist system (artificial myocardium) which is capable of supporting natural contractile functions from the outside of the ventricle without blood contacting surface. In this study, a nano-tech covalent type shape memory alloy fibre (Biometal, Toki Corp, Japan) was employed and the parallel-link structured myocardial assist device was developed. And basic characteristics of the system were examined in a mechanical circulatory system as well as in animal experiments using goats. The contractile functions were evaluated with the mock circulatory system that simulated systemic circulation with a silicone left ventricular model and an aortic afterload. Hemodynamic performance was also examined in goats. Prior to the measurement, the artificial myocardial assist device was installed into the goat's thoracic cavity and attached onto the ventricular wall. As a result, the system could be installed successfully without severe complications related to the heating, and the aortic flow rate was increased by 15% and the systolic left ventricular pressure was elevated by 7% under the cardiac output condition of 3L/min in a goat. And those values were elevated by the improvement of the design which was capable of the natural morphological myocardial tissue streamlines. Therefore it was indicated that the effective assistance might be achieved by the contraction by the newly-designed artificial myocardial assist system using Biometal. Moreover it was suggested that the assistance gain might be obtained by the optimised configuration design along with the natural anatomical myocardial stream line.**

I. Introduction

In general, the artificial ventricular assist systems, such as artificial hearts, were employed for the treatment of the severe heart failure in order to increase the circulation volume. However the complications caused by the hemolysis or thrombosis on the surface of the artificial materials are still outstanding problems in the application of those de-vices to patients. Heart transplantation has also been widely performed as destination therapy for the severe heart failure. But it is limited by donor organ shortages, selection criteria, as well as the cost [1]. And recently, cell transplantation to repair or supplement impaired heart tissue has been reported as an alternative therapy for that [2]. The authors assumed that the essence of the pathophysiological development of severe heart failure was in the decrease in the cardiac contractility. Then an artificial myocardium has been developed using a covalent nano-tech shape memory alloy fibre, which is capable of assisting natural cardiac contraction from out-side of the ventricular wall as shown in Figure 1 [3]. The purpose of this study was to develop a sophisticated artificial myocardium unit, and also to have examined the hemodynamic effects of the myocardial assist system on cardiac function.

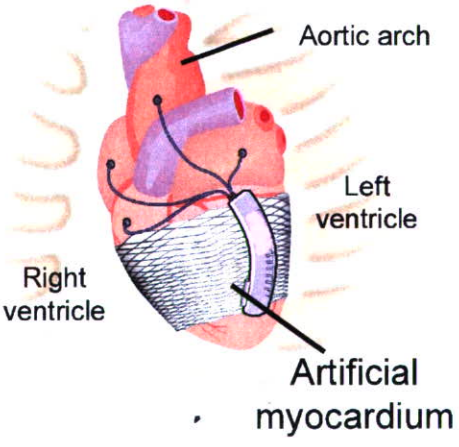

Fig. 1. Schematic illustration of an artificial myocardium attached on the ventricular wall; the synchronous contraction can be achieved according to the natural physiological demand.

This study was supported by Grant in Aid for Scientific Research of Ministry of Health, Labour and Welfare (H17-nano-009), and Ministry of Education, Culture, Sports, Science and Technology (17790938). And this study was partly supported by Grant in Aid for Scientific Research of Pharmaceuticals and Medical Devices Agency and Fujita Memorial Fund of Japan Society for the Promotion of Science..

Y. Shiraishi, T. Yambe, K. Sekine, F. Saijo, H. Liu, S. Konno, S. Nitta are with the Institute of Development, Aging and Cancer, Tohoku University, Sendai 980-8575, Japan (corresponding author to provide phone: +81 22 717 8517; fax: +81 22 717 8518; e-mail: shiraishi@idac.tohoku.ac.jp).

N. Masumoto is with the Department of Mechanical Engineering, Nippon Institute of Technology, Saitama, Japan. Y. Wada, S. Itoh, M. Uematsu, R. Sakata, Y. Park, M. Umezu are with Waseda University, Tokyo, Japan. D. Ogawa, P. Olegario, F. Sato are with the Graduate School of Engineering, Tohoku University, Sendai, Japan. M. Yoshizawa is with the Information Synergy Center, Tohoku University, Sendai, Japan. A. Tanaka is with the Faculty of Symbiotic Systems Science, Fukushima University, Fukushima, Japan. A. Baba and K. Imachi are with Tohoku University Biomedical Engineering Research Organization, Sendai, Japan. K. Tabayashi is with the Graduate School of Medicine, Tohoku University, Sendai, Japan. H. Sasada is with the Graduate School of Agriculture, Tohoku University, Sendai, Japan. T. Fujimoto is with the Shibaura Institute of Technology, Tokyo, Japan. D. Homma is with the Toki Corporation, Tokyo, Japan..

1-4244-0788-5/07/$20.00 ©2007 IEEE

The authors have been developing a totally-implantable artificial myocardial assist device [4]-[6]. The methodologies of the direct ventricular support systems were already reported as direct mechanical ventricular assistance (DVMA) by Anstadt's or other groups, as well as the right ventricular assist device which was invented and reported at IDAC, Tohoku University [7]-[9]. In this study, a design to surround the total heart has been established in order to refrain from the stress concentration by the mechanical assistance, and the hemodynamic performance of the artificial myocardial assist system were examined in a mock circulatory system as well as on animal experiments using goats. And also morphological design approach has been conducted and basic characteristics of the three types of myocardial assist device were examined so that the representation of the anatomical structure of natural myocardial tissue for more sophisticated mechanical assistance from the outside could be achieved.

II. Materials and Methods

A. Artificial Myocardium using Shape Memory Alloy Fibres

The myocardial assist system, as shown in Figure 2, consists of a covalent type shape memory alloy fibre (Biometal®). The diameter of the fibre is 100 microns, and it is contracted by the Joule heating. In general, Ti-Ni alloy is well known as a material with the shape-memory effect[10]-[12]. The fibre material is able to be covered with a silicone –tubing (diameter: 150um). The configuration of the mate-rial was basically constructed by covalent bond, so that it indicated a big strain change by 5 to 10% in length. The linearity of the recovery strain and the changes in electric resistance could be adjusted through the fabrication process, so that the strain of the fibre could be easily controlled by using the digital-servo system without potentiometers.

The layered structures are formed in the ventricular wall from the anatomical point of view as shown in Figure 3, and the effective mechanical blood flow output is achieved by the integrative anisotropic contraction from epi- to endocardium [13].

In this study, the authors developed a prototype artificial myocardium by using the shape memory alloy fibres for the simulation of such natural complicated myocardial tissue stream as shown in Figure 4. And the representation of the myocardial stream on the ventricular wall was performed by the oblique-shaped myocardial assist device.

B. Mock Circulatory Evaluation and Animal Experiments

Contractile function of the device developed was examined onto the originally-designed silicone mock left ventricle (Figure 3). Hydrodynamic evaluation was conducted against the afterload of 80 to 100mmHg without mock ventricular contraction.

Hemodyamic data were also obtained from normal adult

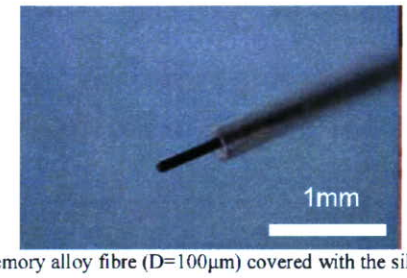

(a) Shape memory alloy fibre (D=100μm) covered with the silicone tubing

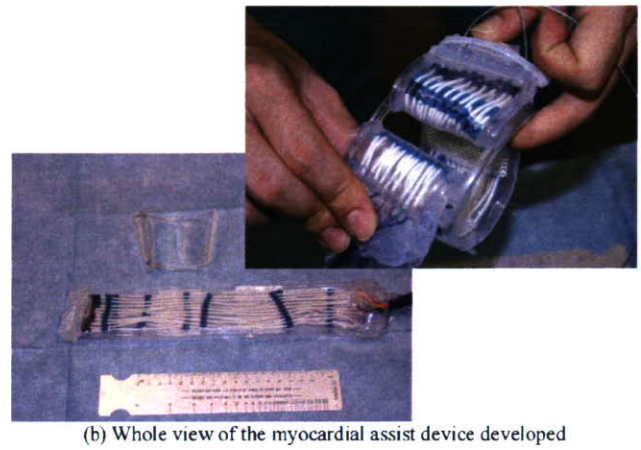

(b) Whole view of the myocardial assist device developed

Fig. 2: The mechanical component of the artificial myocardial actuator (a), and the myocardial assist device of parallel-link structure which was designed to be an active girdle for the ventricular contraction

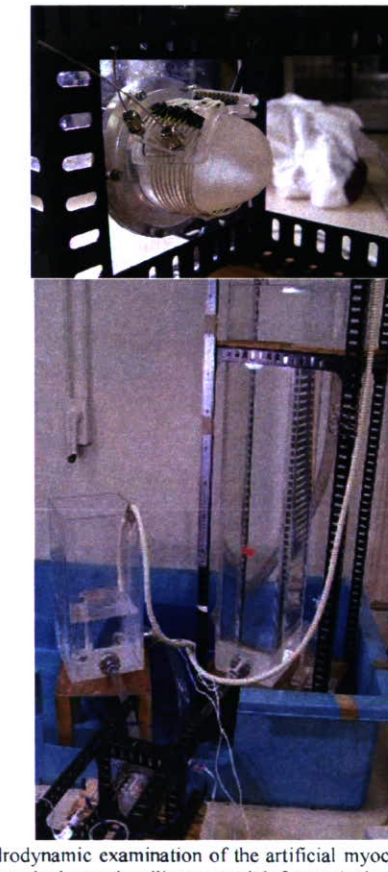

Fig. 3: Hydrodynamic examination of the artificial myocardium (top); the device was attached onto the silicone mock left ventricular model (bottom)

healthy goats, the mean weight of which was 50kg under the normal intubation and general anesthetizing process by 2.5% Fluothane. Prior to the measurement, the artificial myocardial assist device with parallel-linked shape memory alloy fibres was covered with silicone rubber, and it was attached onto the ventricular wall. Left ventricular (LV) pressure was measured by a catheter tip transducer (Millar, SVPC-664A), The sensor was inserted at the left atrial portion through the mitral valve. These hemodynamic data were recorded by a digital recording unit (TEAC, LX-10) and the sampling frequency was 0.5 - 1.5 kHz.

All the animal experiments related to this study were scrutinized and approved by the ethical committee on the animal experiment of the Department of Medicine, Tohoku University, and also the Institute of Development, Aging and Cancer, Tohoku University, 2004-2006.

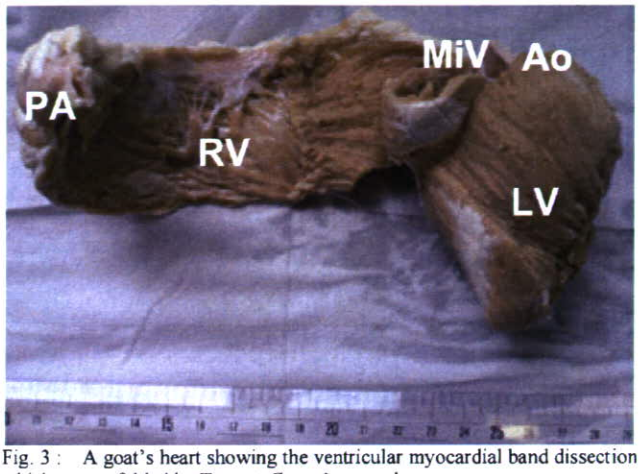

Fig. 3 : A goat's heart showing the ventricular myocardial band dissection which was unfolded by Torrent-Guasp's procedure

III. Results and Discussion

A. Effects of the displacement on the ventricular contraction and design improvement by morphological representation

Basic contraction was achieved to be 5% shortening in each fibre module. Therefore the actual displacement for ventricular assistance together with the acrylic adjustment component was estimated to be over 7%, which was similar to the displacement change obtained from the goat's ventricular surface by using our 3D measurement [14].

As shown in Figure 5, the oblique type which was able to represent the natural morphological myocardial streamline indicated the bigger output of around 5L/min against the after load of 100mmHg in the mock circulatory system.

B. Surgical procedure and hemodynamic effects on the goat's cardiovascular system

In order to achieve the effective reduction of the volume inside of the heart during the systolic phase, the changes of the ventricular wall thickness might be inevitable. Though the concept of supporting cardiac function from outside by using this artificial myocardial assist system does not involve those native thickening function of the heart, the controllable displacement of this device might be useful for more sophisticated cardiac assist.

The myocardial assist device developed was successfully installed into the goat's thoracic cavity without any complications. Hemodynamic waveforms were changed by the mechanical assistance. It was not necessary to remove any costae to install the whole actuator into the thoracic cavity, whereas one rib should be taken away during the surgical procedure of the other electrohydraulic myocardial assist system which had been developed [6]. As the actuator employed for the artificial myocardium itself was so small, the less room in the thoracic cavity might be needed. Moreover,

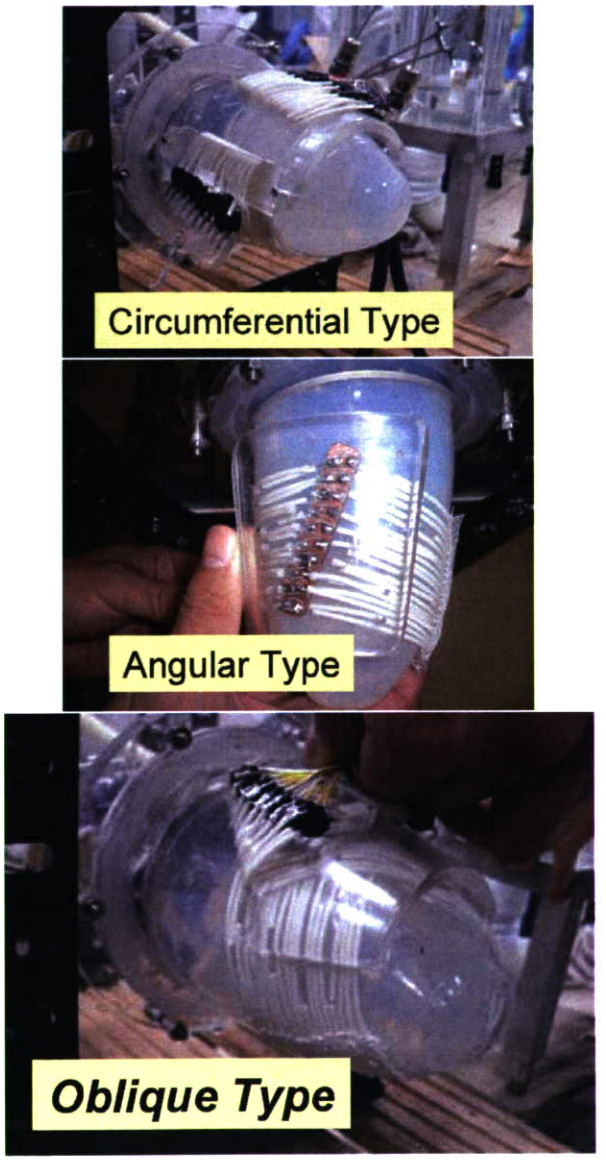

Fig.4: Three different types of the myocardial assist device developed: the oblique type at the bottom could represent the natural oblique stream of myocardial tissue around the left ventricle.

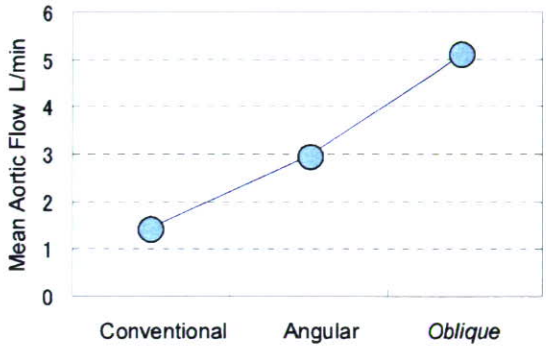

Fig. 5: Changes in mean aortic flow (ventricular model output) obtained from the mechanical circulatory system by using three different configuration types of myocardial assist device.

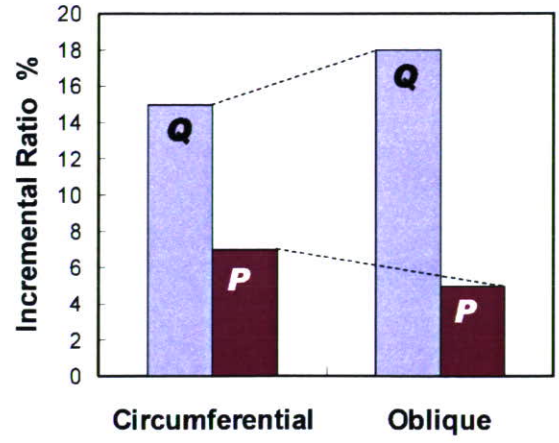

Fig. 6: Changes in the incremental ratio of the hemodynamic data with assistance; P: aortic systolic pressure, Q: aortic flow

the surgical procedure might be simpler compared with other ventricular assist systems. And also the complications, such as thrombosis or hemolysis, would not be caused by this myocardial assist device.

The aortic flow rate was increased by 15% and the systolic left ventricular pressure was elevated by 7% under the cardiac output condition of 3L/min by using the conventional circumferential type. And consequently, the incremental ratio of the left ventricular output was elevated to 18% by using the newly-designed oblique type as showin in Figure 6.

However, any other complications which might have been caused by the operation, such as the disorder of natural autonomic nervous system, were not confirmed in goats yet. As the remarkable increase of the hemodynamic data could be obtained, it was suggested that the effective assistance might be achieved by using this artificial myocardium.

IV. Conclusion

The improvement of an artificial myocardium using the sophisticated covalent shape memory alloy fibres was achieved, which was capable of being installed into the thoracic cavity as the epicardial actuator. As the load of this myocardial system, which was generated by the natural cardiac function, could be estimated by measuring the electrical resistance of the shape-memory alloy fiber, the mechanical myocardial assistance might be effective for heart failure conditions according to the cardiovascular physiological demand.

As our system could assist natural ventricular functions with physiological demand, it might be applied in patients with exertional heart stroke, as well as the cardiac massage at lifesaving emergency for the recovery from ventricular fibrillation.

Acknowledgment

The authors would like to extend their appreciation to Mr. K. Kikuchi and Mr. T. Kumagai for their cooperation in the experiments.

References

[1] Hosenpud JD, et al., "The registry of the international so-ciety for heart and lung transplantation: fifteenth offi-cial report–1998," *J Heart Lung Transplant*, 17, pp. 656–68, 1998

[2] Shimizu T, et al., "Fabrication of pulsatile cardiac tissue grafts using a novel 3-dimensional cell sheet manipulation technique and temperature-responsive cell culture surfaces," *Circ Res*, 90(3), e40, Feb 2002.

[3] Shiraishi Y, et al., "Development of an artificial myocardium using a covalent shape-memory alloy fibre and its cardiovascular diagnostic response" Proc of 2005 IEEE 27th EMBS 0-7803-8740-6/05, 2005

[4] Yambe T, et al., "Addition of rhythm to non-pulsatile circulation," *Biomed Pharmacother*, 58 Suppl 1:S145-9, 2004.

[5] Yambe T, et al., "Artificial myocardium with an artificial baroreflex system using nano technology," *Biomed Pharmacother*, 57 Suppl 1:122s-125s, 2004.

[6] Wang Q, et al., "An artificial myocardium assist system: electrohydraulic ventricular actuation improves myocardial tissue perfusion in goats," *Artif Organs*, 28(9), pp. 853-857, 2004..

[7] Anstadt GL, et al., "A new instrument for prolonged mechanical massage," *Circulation*, 31(Suppl. II), p.43, 1965.

[8] Anstadt M, et al., "Direct mechanical ventricular actuator," *Resuscitation*, 21, pp. 7-23, 1991.

[9] Kawaguchi O, et al., "Dynamic cardiac compression improves contractile efficiency of the heart," *J Thorac Cardiovasc Surg*, 113, pp. 923-31, 1997.

[10] Buehler WJ, Gilfrich J, Wiley KC, "Effect of low-temperature phase changes on the mechanical properties of alloys near composition TiNi," *J Appl Phys*, 34, p.1465, 1963.

[11] Homma D, Miwa Y, Iguchi N, et al., "Shape memory effect in Ti-Ni alloy during rapid heating," *Proc of 25th Japan Congress on Materials Research*, May 1982.

[12] Sawyer PN, et al., "Further study of NITINOL wire as contrctile artificial muscle for an artificial heart," *Carrdiovasc Diseases Bull. Texas Heart Inst* 3, p. 65, 1976.

[13] Torrent-Guasp F, et al., "Structure and function of the heart. Revista Espanola de Cardiologia, 51(2):91-102,1998

[14] Uematsu M, et al., "An innovative approach to evaluate a cardiac functions based on surface measurement", Proc of IEEE 27th EMBS, 0-7803-8740-6/05, 2005.

Proceedings of the 29th Annual International
Conference of the IEEE EMBS
Cité Internationale, Lyon, France
August 23-26, 2007.

Ultrasound Speed and Impedance Microscopy for *in vivo* Imaging

Yoshifumi Saijo, Naohiro Hozumi, Kazuto Kobayashi, Nagaya Okada, Toshimichi Ishiguro, Yoshihiro Hagiwara, Esmeraldo dos Santos Filho and Tomoyuki Yambe

***Abstract*— Ultrasound speed and impedance microscopy was developed in order to develop *in vivo* imaging system. The sound speed mode realized non-contact high resolution imaging of cultured cells. This mode can be applied for assessment of biomechanics of the cells and thinly sliced tissues. The impedance mode visualized fine structures of the surface of the rat's brain. This mode can be applied for intra-operative pathological examination because it does not require slicing or staining.**

I. Introduction

Acoustic microscopy for medicine and biology has been developed for more than twenty years at Tohoku University [1-10]. Application of acoustic microscopy in medicine and biology has three major features and objectives. First, it is useful for intra-operative pathological examination because staining is not required. Second, it provides basic acoustic properties to assess the origin of lower frequency ultrasonic images. Third, it provides information on biomechanics at a microscopic level.

In the present study, ultrasonic microscopy that has two measurement modes, sound speed mode for visualization of single-layered cells and impedance mode for visualization of tissue surface, is proposed.

II. Methods

A. Instruments

Fig. 1 shows the block diagram of the ultrasonic speed and impedance microscopy. An electric impulse was generated by a high speed switching semiconductor. The start of the pulse was within 400 ps, the pulse width was 2 ns, and the pulse voltage was 40 V. The frequency of the impulse covered up to 380 MHz. The electric pulse was used to excite a transducer that had a central frequency of 300 MHz and a sapphire rod as an acoustic lens. The ultrasound spectrum of the reflected ultrasound was broad enough to cover 220-380 MHz (-6dB). The reflections from the tissue was received by the transducer and were introduced into a Windows-based PC (Pentium D, 3.0 GHz, 2GB RAM, 250GB HDD) via a digital oscilloscope (Tektronix TDS7154B, Beaverton, USA). The frequency range was 1 GHz, and the sampling rate was 20 GS/s. Four pulse echo sequences were averaged for each scan point in order to increase the signal-to-noise-ratio.

The transducer was mounted on an X-Y stage with a microcomputer board that was driven by the PC through RS232C. The Both X-scan and Y-scan were driven by linear servo motors.

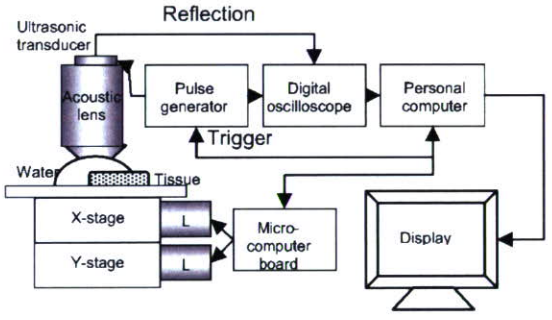

Fig. 1. Block diagram of ultrasonic speed and impedance microscopy

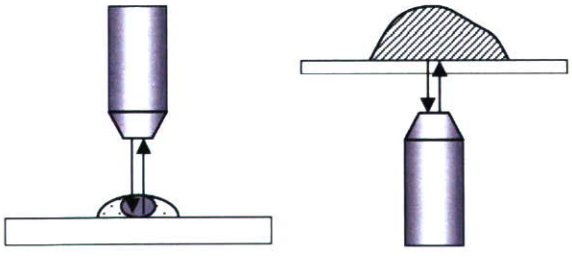

Fig. 2. Schematic illustration of two measurement modes in ultrasonic speed and impedance microscopy. Left: sound speed mode, right: impedance mode

The ultrasonic speed and impedance microscopy has two different modes for observation. Fig. 2 shows the schematic illustration of the relation between the beam propagation and

Manuscript was accepted on June 6, 2007. This work was supported in part by Research Grants from the Ministry of Health, Labor and Welfare for the Research on Advanced Medical Technology (H17-Nano-001) and Grants from New Energy and Industrial Technology Development organization (06001905-0).

Yoshifumi Saijo is with the Institute of Development, Aging and Cancer, Tohoku University, Sendai, 980-8575 Japan (phone: +81-22-717-8514; fax: +81-22-717-8518; e-mail: saijo@ idac.tohoku.ac.jp).

Naohiro Hozumi is with Aichi Institute of Technology, Toyota, Japan. Kazuto Kobayashi, Nagaya Okada and Toshimichi Ishiguro are with Honda Electronics Co. Ltd., Toyohashi, Japan. Yoshihiro Hagiwara is with the Department of Orthopedic Surgery, Graduate School of Medical Science, Tohoku University, Sendai, Japan. Esmeraldo dos Santos Filho and Tomoyuki Yambe are with the Institute of Development, Aging and Cancer, Tohoku University, Sendai, Japan.

1-4244-0788-5/07/$20.00 ©2007 IEEE

the tissue. The left figure shows the sound speed mode for precise imaging (classical acoustic microscopy). The ultrasound propagates through the thinly sliced specimen or cultured cells and reflects at the interface between the specimen and substrate. The right figure shows the impedance mode (acoustic impedance imaging). The ultrasound propagates through the thin plastic plate and is reflected at the interface between plastic and tissue.

B. Tissue Preparation

Sound speed mode is mainly used for visualization of thinly sliced tissues or monolayered cultured cells. In the present study, cultured fibroblast cells were observed by the transmission mode of the ultrasonic imaging system. Fibroblasts were cultured on 35 mm diameter dishes with the Dulbecco's modified Eagle's medium and 10% heat-incubated bovine serum. The incubator was maintained at 37 °C and filled with 95% air and 5% CO_2. After 4days of culture, cells were found to be in the confluent state by inverted microscopy.

Impedance mode can be applied for visualization of tissue surface without thinly slicing the biological tissue. Rats were dissected and the whole brain was removed. A sagittal section of the brain was prepared by a rotor slicer. The specimen was rinsed and preserved in phosphate buffered saline. For optical observation, some adjacent slices were subjected to immuno-histochemical staining against calbindin D-28k.

C. Signal Processing

1) Sound speed Mode

Reflected waveforms are shown in Fig. 3. The waveform at the tissue area is shown in red line and that from substrate is shown in black line. Both signals were captured on the same line in x-scanning.

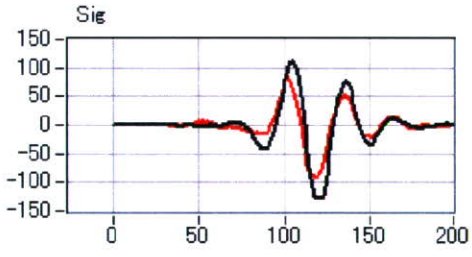

Fig. 3. The waveform at the tissue area (red line) and substrate (black line).

The power spectrum of the reflection at the tissue area is shown in Fig. 4. The spectrum covers the frequency up to 500 MHz. The reflection from the tissue area contains two components. One is from the tissue surface and another from the interface between the tissue and substrate. Frequency domain analysis of the reflection enables the separation of two components [11].

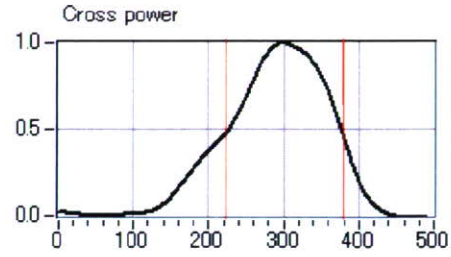

Fig. 4. The power spectrum of the reflection at the tissue area.

Fig. 5 shows the response to a singlet. The left black wave is the reflection from the tissue surface and the right red wave is the reflection from the substrate. These signal processing enables the calculation of tissue thickness and speed of sound.

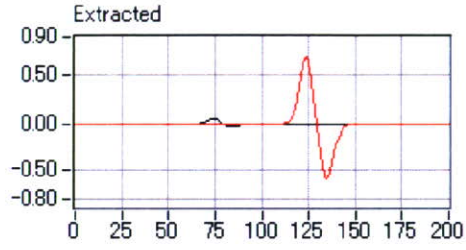

Fig. 5. Response to a singlet. Reflection from he tissue surface (black) and from the substrate (red).

2) Impedance Mode [12]

The target signal is compared with the reference signal and interpreted into acoustic impedance as

$$Z_{target} = \frac{1-\frac{S_{target}}{S_0}}{1+\frac{S_{target}}{S_0}} Z_{sub} = \frac{1-\frac{S_{target}}{S_{ref}} \cdot \frac{Z_{sub}-Z_{ref}}{Z_{sub}+Z_{ref}}}{1+\frac{S_{target}}{S_{ref}} \cdot \frac{Z_{sub}-Z_{ref}}{Z_{sub}+Z_{ref}}} Z_{sub} \cdots (1)$$

where S_0 is the transmitted signal, S_{target} and S_{ref} are reflections from the target and reference, Z_{target}, Z_{ref} and Z_{sub} are the acoustic impedances of the target, reference and substrate, respectively[3].

In case of using water as the reference, its acoustic impedance was assumed to be 1.5 x 10^6 Ns/m^3. On the other hand, in case of using silicon rubber, the acoustic impedance of itself was calibrated, by using water as the standard reference material. In this report, 0.965 x 10^6 Ns/m^3 was used. The acoustic impedance of the substrate was calculated to be 3.22 x 10^6 Ns/m^3, considering its sound speed and density.

III. Results

Fig. 6 and Fig. 7 show the images obtained with the ultrasonic speed and impedance microscopy. Fig. 6 shows the cultured fibroblasts by sound speed mode. The high intensity area at the central part of the cell corresponds to the nucleus (N) and the high intensity area at the peripheral zone corresponds to the cytoskeleton (C) mainly consisted of actin